JMEPEG (2007) 16:200–207
DOI: 10.1007/s11665-007-9032-4

1059-9495/$19.00

The Effects of Stress State and Cavitation on Deformation Stability During Superplastic Forming

Mohammad A. Nazzal and Marwan K. Khraisheh

(Submitted April 20, 2006; in revised form October 22, 2006)

The current available models describing superplastic deformation do not account for a number of important characteristics, leading to the current limited predictive capabilities of deformation and failure. In this work, the effects of cavitation and stress state on deformation stability during superplastic forming are investigated using Finite Element simulations. The simulations are performed using constant strain rate forming and using a proposed optimization approach based on a multiscale failure criterion that accounts for stress state, geometrical necking, and microstructural evolution including grain growth and cavitation. The simulations are conducted for the superplastic copper-based alloy Coronze-638 and the superplastic aluminum alloy Al-5083 which are known to develop significant cavitation during deformation. The results clearly show the importance of accounting for microstructural evolution during superplastic forming, especially when the state of stress is biaxial. Furthermore, the results highlight the effectiveness of the proposed optimization technique in reducing the forming time and maintaining the integrity of the formed parts.

Keywords cavitation, finite element modeling, optimum forming, stability analysis, superplastic forming

1. Introduction

Metal forming industries are constantly looking for ways to increase their productivity and competitiveness by advancing innovative, economical, energy-efficient, and environmentally friendly metal forming techniques. Superplastic Forming (SPF) has a great potential to be one of these exciting advanced forming techniques. SPF is a net shape forming process used with superplastic materials, a unique class of metals that have the ability to exhibit extraordinarily large tensile ductility. SPF offers many advantages over conventional forming operations including weight reduction, greater design flexibility, and the ability to shape hard metals and form complex shapes. However, low production rates and limited predictive capabilities of deformation are among the main obstacles hindering the widespread use of SPF. The current available models describing superplastic deformation do not account for a number of features, leading to the current limited predictive capabilities. These features include anisotropy, microstructural evolution, multiaxiality, and multiscale failure mechanisms. These issues need be addressed in a comprehensive approach, which integrates the mechanics, materials, and manufacturing aspects of superplastic forming process.

Most superplastic materials are shaped by gas pressure forming techniques similar to the techniques used in the glass and plastic industries. Jovane (Ref 1), Cornfield and Johnson (Ref 2), Holt (Ref 3), and Belk (Ref 4) were among the first to present analysis of superplastic blow forming. They attempted to relate the geometry of the formed part to material variables based on uniaxial strain rate hardening relation and considered only forming under constant pressure profiles. Their simple analysis, however, did not agree well with experimental findings. More recently, Dutta and Mukherjee (Ref 5) extended the previous analysis using von Mises flow rules to determine an expression for the forming pressure under constant strain rate of a hemispherical dome. Several investigators used this expression to predict thinning and rupture without success. Since the parts formed using SPF have complex geometries, where analytical expressions for the forming pressure are not available, the attention of researchers was shifted towards finite element (FE) analysis to generate forming pressure profiles (Ref 6-12). The FE simulation of superplastic forming is a complex problem which involves highly non-linear aspects such as large deformation, history-dependent material behavior, and long forming durations. It is important to note that the FE method is an approximate solution to the mathematical model(s) describing structural behavior. Therefore, the FE solution can never be more accurate than what the mathematical model permits. Although the available FE studies on SPF employ different optimization schemes, however, they are based on simple one-dimensional constitutive relations that do not take the main characteristics of superplastic deformation into account. For this reason, it can be said that these models have limited predictive capabilities.

Experimental studies have shown that many superplastic alloys have the tendency to develop cavitation during deformation (Ref 13-16). Cavitation not only limits the superplastic

This article was presented at the AeroMat Conference, International Symposium on Superplasticity and Superplastic Forming (SPF) held in Seattle, WA, June 6-9, 2005.

Mohammad A. Nazzal, and **Marwan K. Khraisheh,** Center for Manufacturing & Department of Mechanical Engineering, University of Kentucky, Lexington, KY 40506-0108. Contact e-mail: khraisheh@engr.uky.edu.

ductility of the material, but also has an adverse effect on the mechanical properties of the formed part. Generally, cavities nucleate at grain boundaries and their subsequent growth and coalescence leads to premature failure (Ref 17). Pilling and Ridley (Ref 13) examined cavitation during superplastic deformation for three different aluminum alloys. They showed that the cavity growth rate under balanced biaxial tension is different than that under uniaxial tension; which means that cavitation is stress state dependent.

The focus of this paper is on two issues: multiaxiality and cavitation. Due to the large deformation associated with superplastic deformation, cavitation plays an important role especially at later stages of deformation. The effects of cavitation on deformation stability during superplastic forming are investigated using FE simulations. The simulations are conducted using standard forming practices (constant strain rate) and using a proposed optimization approach based on a multiscale failure criterion. The results highlight the effects of stress state on deformation. The dominant stress state during superplastic stretching is biaxial and using uniaxial-based models is not adequate especially when large deformation is considered. An overview of the models used in the FE analysis is first given followed by detailed FE analysis.

2. Microstructure-Based Constitutive Model

Based on the continuum theory of viscoplasticity, the constitutive model proposed here accounts for microstructural features including grain growth and cavitation. A simplified form of the model is given by (Ref 18, 19)

$$\dot{\bar{\varepsilon}} = \frac{k}{d^p}\left[\frac{\bar{\sigma}}{(1-f_a)}\right]^{1/m} \quad \text{(Eq 1)}$$

$$d = d_0 + c\bar{\varepsilon} \quad \text{(Eq 2)}$$

where $\bar{\varepsilon}$ and $\dot{\bar{\varepsilon}}$ are the effective strain and strain rate, respectively, $\bar{\sigma}$ is the effective flow stress, m is the strain rate sensitivity index, p is the grain growth exponent, d is the average grain size, d_0 is the initial grain size, f_a is the area fraction of voids, and k and c are material parameters. In order to account for the change in microstructure during deformation, evolution equations for grain size (d) and area fraction of voids (f_a) are used. A simple linear grain growth model similar to the one used by Caceres and Wilkinson (Ref 18) is used here as given by Eq 2. The evolution equation for cavitation is described later. In this work, we consider two superplastic alloys: the copper-based alloy Coronze-638 and the aluminum alloy Al-5083, which are known to develop significant cavitation during deformation. The parameters used in the constitutive model were determined by fitting the model and the evolution equations to the experimental data of Caceres and Wilkinson (Ref 18) for the copper alloy, and Iwasaki et al. (Ref 20) for the aluminum alloy. The results of the model against the experimental data for the copper alloy are shown in Fig. 1 and 2. A very good fit was also obtained for the aluminum alloy. The material parameters used for both alloys are listed in Table 1.

2.1 Cavitation Model

Cavity growth mechanisms can be classified into two categories: diffusional growth and plasticity controlled growth.

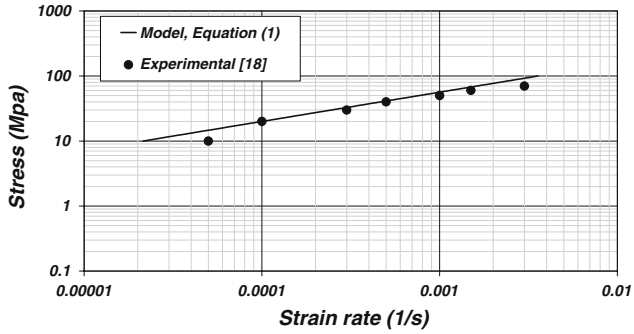

Fig. 1 Stress–strain rate curve for Coronze-638. Model versus experimental data (Ref 18)

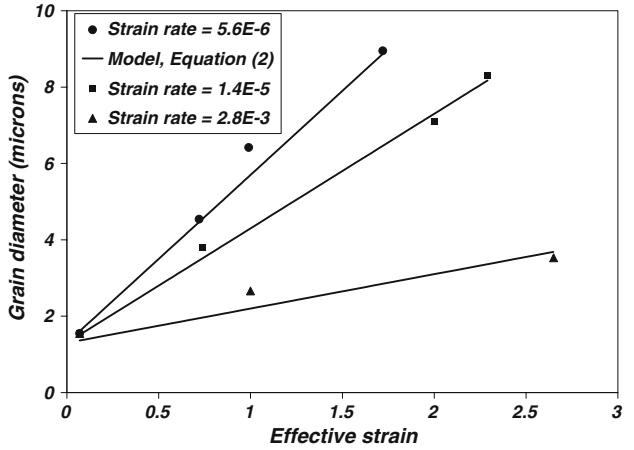

Fig. 2 Grain growth of Coronze-638. Model versus experimental data (Ref 18)

Table 1 List of material properties used in the simulations

Material parameter	Coronze-638	Al-5083
d_0	1.3 μm	13 μm
k	2.19×10^{-21}	1.51×10^{-14}
f_{a_0}	0.01	0.005
m	0.45	0.55
p	2.4	2.0
c	$0.246\times\dot{\varepsilon}^{-0.23}$	$-3.0591 - 1.175\times\log(\dot{\varepsilon})$

Due to the large deformation associated with superplastic deformation, cavitation is primarily controlled by the plastic flow of the surrounding matrix (Ref 17, 21). Plasticity-controlled growth of an isolated and non-interacting cavity is described by the following exponential relation (Ref 22):

$$f_a = f_{a_0}\exp(\psi\bar{\varepsilon}) \quad \text{(Eq 3)}$$

where f_{a_0} is the initial area fraction of voids, and ψ is the void growth parameter that can be expressed as (Ref 17)

$$\psi = \frac{3}{2}\left(\frac{m+1}{m}\right)\sin h\left[2\left(\frac{2-m}{2+m}\right)R\right] \quad \text{(Eq 4)}$$

where R is defined as the ratio between the mean stress (σ_m) and the effective stress ($\bar{\sigma}$)

$$R = \frac{\sigma_m}{\bar{\sigma}} \quad \text{(Eq 5)}$$

3. Multiscale Failure Criterion

In this stability analysis, biaxial stretching of a thin sheet is considered. In order to simplify the analysis, *a priori* neck perpendicular to the loading axis (major principal stress σ_1) is assumed (Ref 23). Based on the incompressibility condition, the following expressions can be derived:

$$\delta\varepsilon_1 = -\frac{\delta A}{A_0} e^{\varepsilon_1} \quad \text{(Eq 6)}$$

$$\delta\dot{\varepsilon}_1 = -\frac{\delta \dot{A}}{A_0} e^{\varepsilon_1} - \frac{\delta A}{A_0}\dot{\varepsilon}_1 e^{\varepsilon_1} \quad \text{(Eq 7)}$$

where A_0 is the initial cross-section area of the sheet and A is the instantaneous cross-section area in the major principle direction. The principal plastic strains ε_1 and ε_2 in the plane of the sheet uniquely characterize the deformation of the sheet and can be defined by the following ratio:

$$\rho = \frac{\varepsilon_2}{\varepsilon_1} = \frac{\dot{\varepsilon}_2}{\dot{\varepsilon}_1} \quad \text{(Eq 8)}$$

where ρ is called the biaxial strain ratio. By the same manner, the stress ratio can be expressed as (Ref 23)

$$\alpha = \frac{\sigma_2}{\sigma_1} = \frac{1+2\rho}{2+\rho} \quad \text{(Eq 9)}$$

The effective stress, effective strain, and effective strain rate can be expressed in terms of the principal values as follows (Ref 23):

$$\bar{\sigma} = b\sigma_1, \bar{\varepsilon} = a\varepsilon_1, \dot{\bar{\varepsilon}} = a\dot{\varepsilon}_1 \quad \text{(Eq 10)}$$

where 'a' and 'b' are functions of the biaxial strain ratio (ρ) and are given by the following expressions (Ref 23):

$$a = \sqrt{\frac{4}{3}(1+\rho+\rho^2)} \quad \text{(Eq 11)}$$

$$b = \frac{1}{(2+\rho)}\sqrt{3(1+\rho+\rho^2)} \quad \text{(Eq 12)}$$

The condition for stable plastic deformation as defined by Hart is used here (Ref 24)

$$\left(\frac{d\dot{A}}{dA}\right) \leq 0 \quad \text{(Eq 13)}$$

Although there has been some controversy regarding the applicability of Hart's definition on stable plastic deformation, Nichols (Ref 25) presented a detailed review on the subject of plastic instabilities and compared the results of the more recent analyses to Hart's analysis, and concluded that the results obtained by these more recent studies are already implicitly contained in Hart's theory.

Based on Hart's condition for stable deformation, Eq 1-3 are solved along with Eq 6-12 to obtain a new stability criterion that accounts for both geometrical instabilities and microstructure aspects for a biaxial loading case. This criterion has the following form at the onset of instability (Ref 26)

$$a\gamma^* + m + a\zeta^* = 1 \quad \text{(Eq 14)}$$

where

$$\gamma^* = \frac{\dot{d}}{\dot{\bar{\varepsilon}}^2}\left(\frac{\partial\dot{\bar{\varepsilon}}}{\partial d}\right)_{\bar{\sigma},f_a}, \quad m^* = \frac{\bar{\sigma}}{\dot{\bar{\varepsilon}}}\left(\frac{\partial\dot{\bar{\varepsilon}}}{\partial\bar{\sigma}}\right)_{d,f_a}, \quad \zeta^* = \frac{\psi f_a}{\dot{\bar{\varepsilon}}}\left(\frac{\partial\dot{\bar{\varepsilon}}}{\partial f_a}\right)_{\bar{\sigma},d}$$

The first term in the above equation corresponds to strain hardening due to grain coarsening, the second term corresponds to strain rate sensitivity and the third term represents the influence of cavitation. Figure 3 shows the effect of biaxial strain ratio (ρ) on the forming path for the copper alloy. It is important to note that this stability criterion is general and can be used with any constitutive relation expressed as $\dot{\bar{\varepsilon}} = \dot{\bar{\varepsilon}}(\bar{\sigma}, \bar{\varepsilon}, d, f_a)$. The contribution of grain growth and cavitation depends on their evolution equations and on the way they are represented in the constitutive relation.

4. Discussion and Results

The commercial finite element code ABAQUS is used to perform the simulations. Two user-defined subroutines are developed to define the material viscoplastic behavior. A built-in pressure control algorithm aimed at obtaining a practical load curve at low computational cost is used in the analysis. Details on the development and validation of this algorithm can be found elsewhere (Ref 27).

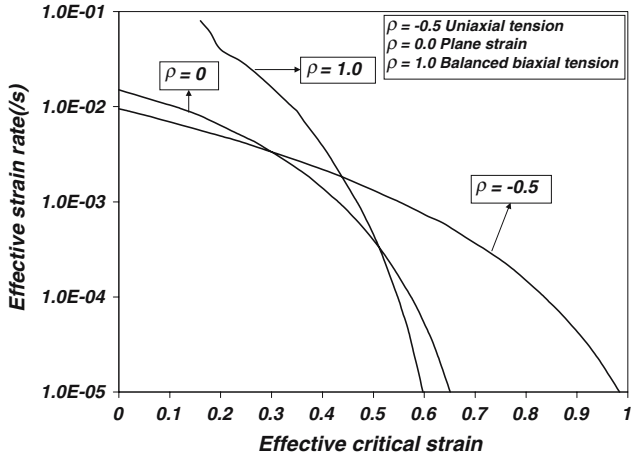

Fig. 3 Effect of biaxiality ratio on the optimum forming path for Coronze-638

First, two simulation runs are conducted to study the effects of biaxial strain ratio on the stability of superplastic forming. Then we present a comparison between two pressure control schemes, i.e., constant strain rate forming scheme and variable strain rate forming scheme based on the multiscale failure criterion that was developed earlier (Ref 26), for two different geometries. It is important to note that the stability criterion and FE simulations are based on experimentally validated and calibrated constitutive relations with microstructural evolution (Eq 1-3). The flow stress results from FE simulations match the experimental flow stress results reported by Caceres and Wilkinson (Ref 18) and Iwasaki et al. (Ref 20).

In our previous work (Ref 28), optimum variable strain rate forming paths using a uniaxial-based multiscale stability analysis were derived and used to develop variable strain rate forming pressure profiles. However, since the dominant stress state during superplastic stretching is biaxial, the new biaxial stability criterion Eq 14 is used in this work to generate optimum variable strain rate paths that account for stress biaxiality.

4.1 Effects of Stress State

Figure 4 shows the finite element model for simulating superplastic forming of Coronze-638 sheet into a dome at 550 °C. The reason for selecting this simple geometry is that the stress state at the pole of the dome is known to be balanced biaxial which allows us to compare with uniaxial results and examine the effect of stress state on the deformation. The load is controlled according to the strain rate found at the polar region of the dome. The free-forming region of the sheet is 7.62 cm in diameter, with a 0.39 cm flange around it. The initial thickness of the sheet is 0.198 cm. Due to symmetry, a quarter of the blank is modeled using 885 quadrilateral fully integrated bilinear membrane elements. The sheet is clamped along the circumference and symmetric boundary conditions are applied along the axis of symmetry.

From Fig. 3, it is observed that during the initial stages of deformation (low strains), more stable deformation is achieved for higher biaxial strain ratios. In other words, higher critical strains can be achieved for the same strain rate when the biaxial strain ratio is increased, which allows for faster forming while maintaining stable deformation. However, at later stages of deformation, the highest state of stable deformation is achieved for the uniaxial loading case ($\rho = -0.5$) and faster forming can be conducted while maintaining stable deformation. To check the validity of this observation, two simulation runs for the blow-forming of a dome are conducted. In the first run, a uniaxial-based FE model is used, and the load is controlled according to the variable strain rate path for the uniaxial loading case ($\rho = -0.5$) shown in Fig. (3). In the second run, the FE model accounts for biaxiality and the load is controlled according to the path derived for the balanced biaxial case ($\rho = 1.0$); which is the actual state of stress at the pole. The results of the two runs at two different stages of deformation are evaluated at effective strains of 0.235, i.e., early deformation stage, and 0.51, i.e., later deformation stage. The nominal thickness distribution and area fraction of voids of the formed sheets along a radial line that passes through the pole are shown in Fig. 5 and 6, respectively. The nominal thickness distribution does not take into account the amount of cavitation generated during deformation. Hence, the term nominal is used. At an effective strain of 0.235 at the pole, it is observed that the nominal sheet thickness is almost the same for the uniaxial and biaxial-based models. Although the area fraction of voids at this strain is slightly higher for the biaxial-based model, the deformation is still stable. This is because an area fraction of voids of 0.029 is not considered to be significant and will not have a remarkable influence on deformation stability. In addition, the forming time for the biaxial case is 22 s, which is less than that for the uniaxial case (50 s). Therefore, it is

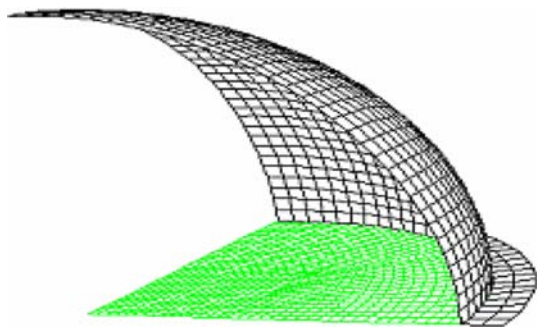

Fig. 4 FE model for simulating gas blow forming of the dome

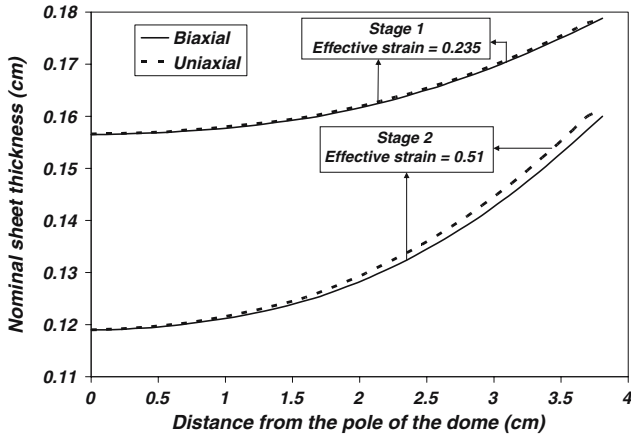

Fig. 5 Variation of nominal sheet thickness for different biaxial strain ratios

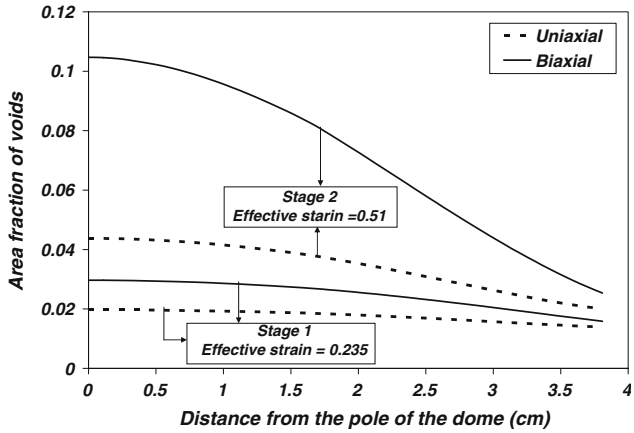

Fig. 6 Variation of area fraction of voids for different biaxial strain ratios

Table 2 Summary of the results for the uniaxial and biaxial-based models for the dome

		Uniaxial case	Biaxial case
$\varepsilon = 0.235$	Forming time (s)	50	22
	Minimum thickness (cm)	0.156	0.156
	Maximum area fraction of voids	0.0198	0.029
$\varepsilon = 0.51$	Forming time (s)	232	3260
	Minimum t thickness (cm)	0.119	0.118
	Maximum area fraction of voids	0.045	0.11

observed that the biaxial case is more stable at this stage. This observation can be explained as follows: in the early stages of deformation, stability is dominated by geometrical considerations since microstructural features need more time to evolve and contribute to deformation and failure. As a result, any addition of biaxial tensile load in the early stages of deformation tends to delay the onset of necking perpendicular to the major stress axis. Hence and in order to maintain stable deformation, more time was needed for the uniaxial case when compared with the biaxial case during the early stages of deformation.

The results at late stages of deformation are different. To reach an effective strain of 0.51 at the pole while maintaining stable deformation, it took 3260 s for the biaxial case and only 232 s for the uniaxial case. This remarkable difference in forming time can be explained by the results shown in Fig. 6. The area fraction of voids for the biaxial-based model is high (0.11) compared to that for the uniaxial-based model (0.045). This high area fraction of voids has a significant influence on deformation stability and slower forming is needed to avoid premature failure. These results clearly highlight the importance of accounting for the actual stress state, since it has profound influence on the microstructural evolution, especially for large deformations. In actual sheet metal forming operations, the state of stress is biaxial and using uniaxial-based models may provide misleading results especially when large deformation is considered. A summary of the results for the biaxial and uniaxial-based models for the blow forming of a dome is given in Table 2.

4.2 Variable Strain Rate Versus Constant Strain Rate Forming

One of the critical aspects of superplastic forming analysis is to determine the pressure–time history required to form the component as fast as possible without causing material failure. The practice of maintaining the target strain rate at a constant value that is the optimum for superplasticity typically leads to very slow forming. Khraisheh and Zbib (Ref 29) have shown experimentally that using a variable strain rate forming approach can reduce the forming time without compromising the uniformity of the formed part. The approach followed in that study was based on experimental observations and not on scientific basis. However, the results presented in Fig. 3 are derived from a multiscale stability criterion that takes into account both geometrical necking and microstructural evolution, which can provide the scientific framework for developing the optimum variable strain rate forming paths. To demonstrate the effectiveness of the modified stability criterion that uses a variable strain rate path, three simulation runs were conducted according to the following load control schemes:

1. The forming pressure profile is based on a constant strain rate of (10^{-2} s^{-1}).
2. The forming pressure profile is based on an optimum variable strain rate path derived from the multiscale stability criterion. The path with ($\rho = 1.0$) will be implemented in this analysis.
3. The forming pressure profile is based on a constant strain rate of (10^{-4} s^{-1}).

In order to have meaningful comparisons, the forming process is considered to be completed when the dome height reaches 2.2 cm and the FE model accounts for biaxiality.

Table 3 shows the forming time and thinning factor at different forming strain rates for the dome. The thinning factor is defined as the ratio between the nominal thickness of the sheet at the pole of the dome and the average nominal sheet thickness (Ref 2). Higher thinning factors indicate more uniform thickness distribution. The nominal thickness distribution and the area fraction of voids of the formed sheets along a radial line that passes through the pole are shown in Fig. 7 and 8, respectively. From Fig. 7, it is observed that the sheet formed at the lowest strain rate (10^{-4} s^{-1}) shows the most uniform thickness distribution and minimum localized thinning. However, 4146 s are needed to form the part. Using the (10^{-2} s^{-1}) strain rate, forming takes only 48 s; but the resulting thickness distribution is highly non-uniform, and the localized thinning is severe at the pole. When the optimum strain rate path is used, not only the forming time is reduced from 4146 to 601 s, but also the uniformity of the sheet thickness is maintained and compares very well with the one obtained using the low target strain rate. Similarly, the variable strain rate scheme successfully reduced the area fraction of voids without compromising the forming time as shown in Fig. 8.

Figure 9 shows the variation of the dome height with forming time. From this figure, it is shown that the proposed

Table 3 Forming time and thinning factor at different strain rates for the dome

	Strain rate, 10^{-2} s^{-1}	Optimum	Strain rate, 10^{-4} s^{-1}
Forming time(s)	48	601	4146
Thinning factor	0.73	0.84	0.85

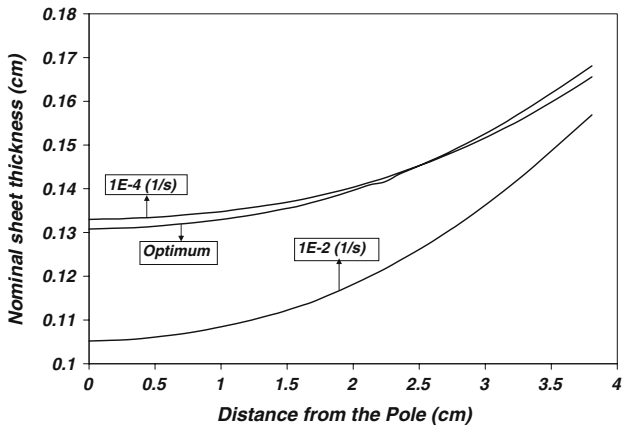

Fig. 7 Variation of nominal thickness at different strain rates

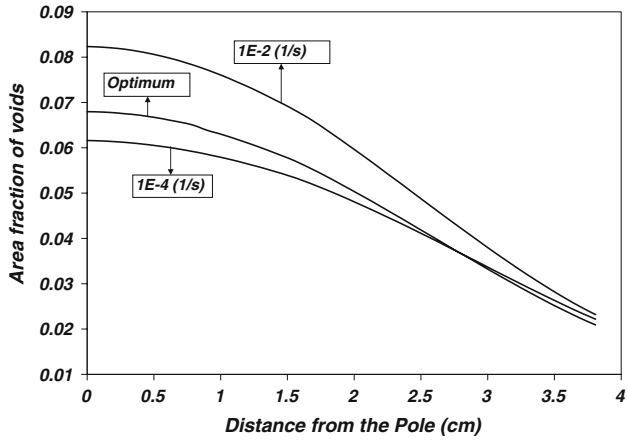

Fig. 8 Variation of area fraction of voids at different strain rates

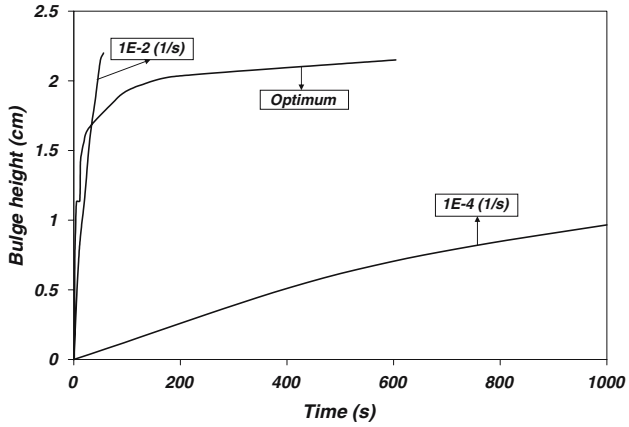

Fig. 9 Variation of the bulge height with time at different strain rates

optimum approach acts as a smart control that adjusts the deformation speed according to the actual material behavior during deformation. Initially, the dome height increases rapidly and as deformation continues, the strain rate is adjusted to lower values in order to avoid instable deformation due to geometrical necking and microstructural evolution (grain growth and cavitation).

4.2.1 Effective Thickness. To account for the evolution of damage in the thickness distribution, we define the effective thickness (t_{eff}) as

$$t_{\text{eff}} = (1 - f_{\text{a}}) \times t_{\text{nom}} \qquad \text{(Eq 15)}$$

where t_{nom} is the nominal sheet thickness. Figure 10 shows a comparison between the nominal and effective sheet thickness distributions for different forming strain rates. From Fig. 10, it is seen that the polar region is highly affected (much thinner) when damage evolution is accounted for in calculating the thickness distribution. This is due to the fact that the minimum nominal thickness and the maximum area fraction of voids occur at the pole. This result clearly shows the importance of accounting for microstructural evolution when calculating the thickness distribution in the formed parts since it directly affects the mechanical integrity and may require changes to the design specifications.

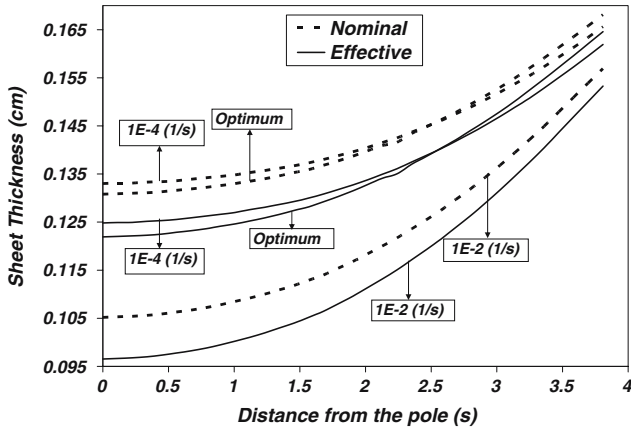

Fig. 10 Variation of nominal and effective sheet thickness at different strain rates

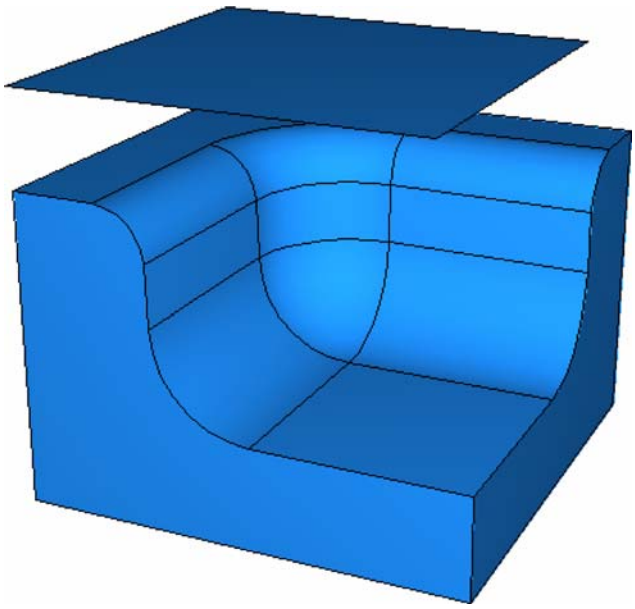

Fig. 11 Die-sheet geometry for simulating superplastic gas blow forming of a box

5. Application

After the influence of microstructural evolution and stress state on deformation stability are demonstrated, we formed a box made of Al 5083 alloy with a biaxial strain ratio different than that of the dome. Figure 11 shows the die-sheet geometry for simulating superplastic forming of a sheet into a box. The final dimensions of the box are 15.2 cm long by 15.2 cm wide by 5.08 cm deep with a 1.27 cm flange around it. The initial dimensions of the blank are 20 cm by 20 cm, and the thickness is 0.1 cm. The isotropic Coulomb friction model provided by ABAQUS with a friction coefficient ($\mu = 0.1$) is used to account for surface interaction between the die and the sheet. After preliminary runs were performed, we observed that both the maximum localized thinning and maximum strain in the sheet occur at the box's bottom corner. Therefore, the pressure is controlled on the basis of the maximum equivalent creep strain rate found in the bottom corner of the box. In addition, it

was found that the biaxial strain ratio in this critical region oscillates between 0.8 and 1.0.

To show the effectiveness of the optimization technique and the importance of accounting for microstructural evolution and biaxiality during deformation, three simulations runs were conducted. In the first run, a uniaxial-based FE model is used and the maximum equivalent strain rate is set to 10^{-4} s^{-1}. In the second run, a biaxial-based FE model is used and the maximum equivalent strain rate is set to 10^{-4} s^{-1}. In the third run, a biaxial-based FE model is used and the forming pressure profile is based on an optimum variable strain rate path, derived for Al 5083 alloy from the multi-scale stability criterion, with ($\rho = 0.9$) since the biaxial strain ratio in this critical region oscillates between 0.8 and 1.0. The forming times for the three runs are as follows: it took 8855 s to form the part using the uniaxial-based model at a constant strain rate of 10^{-4} s^{-1}, 8950 s to form the part with the biaxial-based model at a constant strain rate of 10^{-4} s^{-1}, and 1738 s to form the part using the optimum strain rate path. Figure 12 and 13 respectively, show the damage distribution and the effective sheet thickness distribution for the three runs. The results show again the ability of the optimization technique to reduce the forming

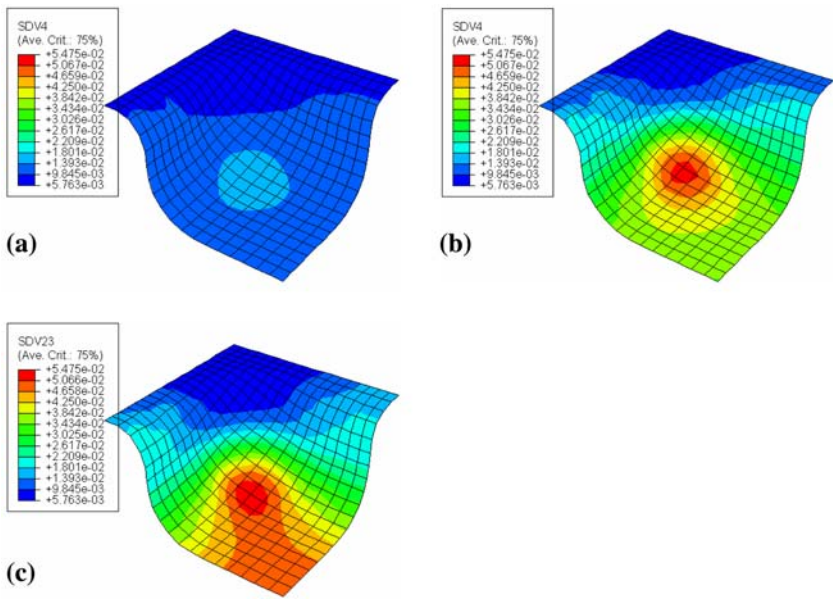

Fig. 12 (a) Damage distribution using the uniaxial-based model for constant strain rate forming at 10^{-4} s^{-1}. (b) Damage distribution using the biaxial-based model for constant strain rate forming at 10^{-4} s^{-1}. (c) Damage distribution for the optimum forming path

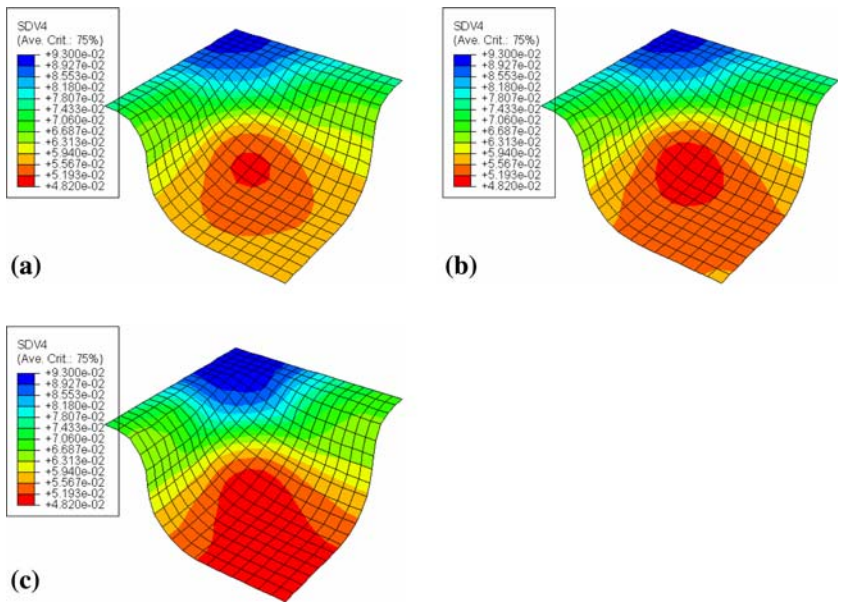

Fig. 13 (a) Effective thickness distribution using the uniaxial based model for constant strain rate forming at 10^{-4} s^{-1}. (b) Effective thickness distribution using the biaxial based model for constant strain rate forming at 10^{-4} s^{-1}. (c) Effective thickness distribution for the optimum forming path

time without compromising the integrity of the formed part and the importance of accounting for microstructural evolution and biaxiality during deformation.

6. Conclusions

A detailed finite element analysis for simulating superplastic forming is presented using experimentally validated microstructure-based constitutive model along with grain growth and cavitation evolution equations. The analysis provides useful and new information on the effects of stress state and cavitation on deformation stability. The proposed optimum variable strain rate deformation paths have resulted in a significant reduction in the forming time without compromising the integrity of the formed part. Finally, for design specifications of superplastically formed sheets, the effective thickness must be used since significant deviations from the nominal thickness were observed. This is particularly important because the stress state is biaxial and the damage evolution is significant.

Acknowledgment

The support of the National Science Foundation, CAREER Award # DMI-0238712, is acknowledged.

References

1. F. Jovane, An Approximate Analysis of the Superplastic Forming of a Thin Circular Diaphragm: Theory and Experiments, *Int. J. Mech. Sci.*, 1968, **10**(10), p 403–427
2. G.E. Cornfield and R.H. Johnson, The Forming of Superplastic Sheet Metal, *Int. J. Mech. Sci.*, 1970, **12**, p 479–490
3. D.L. Holt, Analysis of the Bulging of Superplastic Sheet by Lateral Pressure, *Int. J. Mech. Sci.*, 1970, **12**, p 491–497
4. J.A. Belk, A Quantitative Model of the Blow Forming of Spherical Surfaces in Superplastic Sheet Metal, *Int. J. Mech. Sci.*, 1975, **17**, p 505–511
5. A. Dutta and A.K. Mukherjee, Superplastic Forming: An Analytical Approach, *Mater. Sci. Eng.*, 1992, **A157**, p 9–13
6. X.D. Ding, H.M. Zbib, C.H. Hamilton, and A.E. Bayoumi, On the Optimization of Superplastic Blow-Forming Processes, *J. Mater. Eng. Perform.*, 1995, **4**(4), p 474–485
7. L. Carrino and G. Guiliano, Modeling of superplastic blow forming, *Int. J. Mech. Sci.*, 1997, **39**(2), p 193–199
8. X.L. Xing and Z.R. Wang, Finite Element Analysis and Design of Thin Sheet Superplastic Forming, *J. Mater. Process. Technol.*, 1997, **68**, p 1–7
9. M.A. Khaleel, K.I. Johnson, C.H. Hamilton, and M.T. Smith, Deformation Modeling of Superplastic AA-5083, *Int. J. Plasticity*, 1998, **14**(10-11), p 1113–1154
10. A. Huang, M.J. Cardew-Hall, and A. Lowe, Sheet Thickness Optimization of for Superplastic forming of Engineering Structures, *ASME J. Manuf. Sci. Eng.*, 2000, **122**(1), p 166–173
11. Y.H. Kim, J.M. Lee, and S.S. Hong, Optimal Design of Superplastic Forming Processes, *J. Mater. Process. Technol.*, 2001, **112**, p 166–173
12. L.C. Chung and J.H. Cheng, The Analysis of Instability and Strain Concentration during Superplastic Deformation, *Mater. Sci. Eng.*, 2001, **A308**, p 153–160
13. J. Pilling and N. Ridley, Effect of Hydrostatic Pressure on Cavitation in Superplastic Aluminum Alloys, *Acta Metall.*, 1986, **34**(4), p 669–679
14. M.B. Taylor, H.M. Zbib, and M.A. Khaleel, Damage and Size Effect during Superplastic Deformation, *Int. J. Plasticity*, 2002, **18**(3), p 415–442
15. D.H. Bae and A.K. Ghosh, Cavity Growth in a Superplastic Al–Mg Alloy: II. An Improved Plasticity Based Model, *Acta Mater.*, 2002, **50**(5), p 1011–1029
16. N. Chandra, M.K. Khraisheh, and P. Kalu, Effect of Stress Sate on the Cavitation Behavior of AL 5083 Superplastic Behavior, *Mater. Sci. Forum*, 2005, **475–479**, p 2931–2936
17. J. Pilling and N. Ridley, *Superplasticity in Crystalline solids*. The Institute of Metals, London, UK, 1989, p 102–157
18. C.H. Caceres and D.S. Wilkinson, Large Strain Behavior of a Superplastic Copper Alloy Deformation, *Acta Metall.*, 1984, **32**, p 415–422
19. N.V. Thuarmalla and M.K. Khraisheh, Effects of Microstructural Evolution on the Stability of Superplastic Deformation. *Proceedings of the Second MIT Conference on Computational Fluid and Solid Mechanics*, Vol 1, 2003, p 683–686
20. H. Iwasaki, K. Higashi, S. Tanimura, T. Komatubara, and S. Hayami, Superplastic Deformation Charactristics of 5083 Aluminum Alloy, *Superplasticity in Advanced Materials*, S. Hori, M. Tokizane, and N. Furushiro, Eds., The Japan Society for Research on Superplasticity, 1991, p 447–452
21. H. Iwasaki, S. Hayami, K. Higashi, and S. Tanimura, Instability of Superplastic Aluminum Alloys, *Materials Research Society Symposium Proceedings*, Vol 196, 1990, p 233–238
22. M.J. Stowell, Cavity Growth and Failure in Superplastic Alloys, *Metal Sci.*, 1983, **17**, p 92–98
23. X.D. Ding, H.M. Zbib, C.H. Hamilton, and A.E. Bayoumi, On the Stability of Biaxial Stretching with Application to the Optimization of Superplastic Blow-Forming, *J. Eng. Mater. Technol. ASME Trans.*, 1997, **119**, p 26–31
24. E.W. Hart, Theory of the Tensile Test, *Acta Metall.*, 1976, **15**, p 351–355
25. F.A. Nichols, Plastic Instabilities and Uniaxial Tensile Ductilities, *Acta Metall.*, 1980, **28**, p 663–673
26. N.V. Thuramalla and M.K. Khraisheh, Multiscale-Based Optimization of Superplastic Forming, *Transactions of NAMRI/SME*, Vol 32, 2004, p 637–643
27. R. Hambli, A. Potiron, F. Guerin, and B. Dumon, Numerical Pressure Prediction Algorithm of Superplastic Forming Process using 2D and 3D Models, *J. Mater. Process. Technol.*, 2001, **112**, p 83–90
28. M.A. Nazzal, M.K. Khraisheh, and B. Darras, Finite Element Modeling and Optimization of Superplastic Forming Using Variable Strain Rate Approach, *ASM J. Mater. Eng. Perform.*, 2004, **13**(6), p 691–699
29. M.K. Khraisheh and H.M. Zbib, Optimum Forming Loading Paths for Pb–Sn Superplastic Sheet Materials, *ASME J. Eng. Mater. Technol.*, 1999, **121**, p 341–345